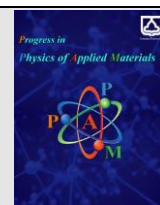




Semnan University

journal homepage: <https://ppam.semnan.ac.ir/>

The effect of calcination temperature on the X-ray peak broadening of t-CuFe₂O₄

M. Choupani, A. Gholizadeh*

School of Physics, Damghan University, Damghan, Iran

ARTICLE INFO

Article history:

Received: 16 May 2021

Revised: 8 June 2021

Accepted: 4 July 2021

Keywords:

CuFe₂O₄

spinel structure

Crystallite sizes

Lattice micro-strain

Isotropic line broadening

ABSTRACT

CuFe₂O₄ ferrite was synthesized by citrate precursor and then calcined at 800, 900, and 1000 °C. Structural properties showed that the X-ray diffraction patterns of the samples could be easily indexed to tetragonal CuFe₂O₄ ferrite with the spatial group the *I* 41/*AMD*. As the calcination temperature increased, the larger Cu²⁺ ion at the tetragonal site substituted the smaller Fe³⁺ ion at the octahedral site. The half-width of X-ray diffraction peaks can be affected by several factors such as instrumentation, crystallite size, and lattice microstrain broadening. The results of crystallite size and Microstrain estimated by different methods for the samples show that the Size-strain Plot method is more accurate, the value of R² is close to 1 and all data points touch the fitting line better than other methods. The results showed that the increase in crystal size with calcination temperature could be mainly attributed to the increase of stretching microstrain.

1. Introduction

Among all magnetic nanomaterials, spinel ferrites have recognizable magnetic, electrical, and optical properties. Their magnetic and electrical properties such as high saturation magnet as well as high dielectric properties, low eddy current losses, initial permeability enable a wide range of applications for spinel ferrites [1].

Spinel ferrites have a general formula $(M_{\delta}Fe_{1-\delta})[M_{1-\delta}Fe_{1+\delta}]O_4$; here, δ is the cation distribution factor, which illustrates the fraction of tetrahedral (A-) sites occupied by divalent metal (M²⁺) cations. The round and square brackets denote the tetrahedral (A) and octahedral (B) interstitial sites, and M is the divalent (Cu²⁺, Mn²⁺, Co²⁺, Ni²⁺, Zn²⁺, etc.) and Fe is a trivalent (Fe³⁺) metal cation occupying the FCC lattice formed by O²⁻ anions. Among spinel ferrites, CuFe₂O₄ spinel ferrite has received great attention as its magnetic properties can be tuned by cation distribution at octahedral and tetrahedral sites [2].

So far, a wide range of methods have been used to synthesize ferrite spinel materials including solid-state reaction, solvothermal method, chemical vapor deposition, reverse microwave microemulsion synthesis, microwave method, one-step reflex strategy, Metal-organic-framework-engaged synthetic strategy, and the sol-gel method, etc. Among them, the sol-gel synthesis method shows the significant advantages of low external energy

consumption, inexpensive precursors and homogeneous powders with high reactivity [3].

Both preparation techniques and crystal imperfections can affect the properties of nanostructures. Bragg's equation assumes the crystal is perfect and infinite and the incident beam is perfectly parallel and monochromatic. Actual experimental conditions are different from these leading to various kinds of deviations from Bragg's condition. Peaks are not 'd' curves and peaks are broadened. There are also deviations from the assumptions involved in generating powder patterns. For example, in a powder sample, if the crystallite size is smaller than 0.5 mm, there is an insufficient number of planes to build up a sharp diffraction pattern and then peaks are broadened. Both crystallite size and lattice microstrain have affect on Bragg's peaks by increasing the peak width, intensity and shifting the 2θ peak position [4, 5]. Therefore, the two main properties extracted from peak width analysis are the crystallite size and lattice strain. The half-width of the experimentally measured breadth (β) can be influenced by instrumental (β_I), the crystallite size (β_C), lattice microstrain (β_S), stacking fault (β_{SF}), and other defects. Consequently:

$$\beta(\text{FWHM}) = \beta_I + \beta_C + \beta_S + \beta_{SF} + \dots \quad (1)$$

The diffraction peak that we see is a result of various broadening 'mechanisms' as shown in Fig. 1.

* Corresponding author. Tel.: +989120816781

E-mail address: gholizadeh@du.ac.ir

In this paper, we analyze the peak of XRD expansion of calcined CuFe_2O_4 at 800, 900, and 1000 °C using an X'pert commercial package. A comparative study of the mean crystallite size and microstrain of the samples estimated by different models of Williamson Hall (W-H) analysis, size-strain plot (SSP), and Halder-Wagner (H-W) is reported. The microstrain originates from the lattice deformation of the CuFe_2O_4 ferrite lattice due to different calcination temperatures. The results of crystallite sizes obtained by these methods are compared with Scherrer methods.

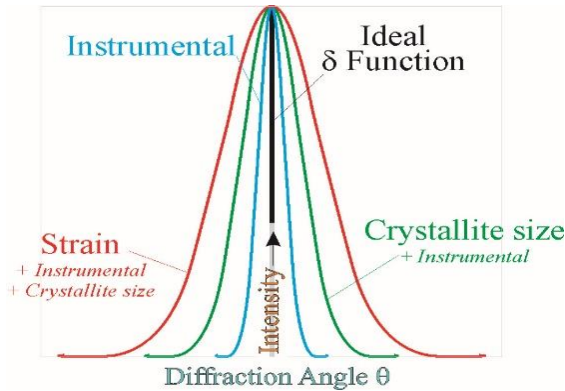


Fig. 1. The contribution of the instrumental (β_i), the crystallite size (β_c), the lattice microstrain (β_s) broadening on diffraction peak

2. Sample synthesis

2.1. Sample synthesis

To prepare the copper ferrite by a citrate method, stoichiometric proportions of $\text{Cu}(\text{NO}_3)_2 \cdot 6\text{H}_2\text{O}$ and $\text{Fe}(\text{NO}_3)_3 \cdot 9\text{H}_2\text{O}$ were completely dissolved in a minimum amount of deionized water. The molar ratio of copper nitrate to iron nitrate was 1:2. Then the solution of citric acid ($\text{C}_6\text{H}_8\text{O}_7$) was used as a chelating agent and added into the solution under stirring. The mole ratio of the citric acid to the total metal ions was 1:1. The mixture was stirred for 1 h at room temperature and then heated at 80 °C until a viscous gel was obtained. The resultant gel was dried at 200 °C for 12 h and a precursor was obtained. Finally, the precursor was annealed at different temperatures of 800, 900, and 1000 °C for 2 h to obtain the products. The synthesized copper ferrite powder samples are designated as CuF1, CuF2, and CuF3 according to annealing temperatures of 800, 900, and 1000 °C, respectively.

2.2. Geometric characterization

X-ray diffraction (XRD) analysis was used to obtain the crystal structure of the material. The XRD pattern was recorded using a Bruker AXS D8 ADVANCE diffractometer with $\text{Cu-K}\alpha$ radiation in the range of $2\theta = 10\text{-}80^\circ$ at room temperature. Fullprof program and X'pert package were used to analyze XRD data. XRD profile analysis is a simple and powerful method for evaluating crystal size and lattice microstrain. Here, two factors can determine the peak Bragg amplitude, including crystal size-dependent expansion (β_c) and microstrain-dependent expansion (β_s), which is added to the instrument-dependent expansion.

3. Results and Discussion

3.1. The XRD analysis

The X-ray diffraction patterns of CuFe_2O_4 ferrite powder samples annealed at different temperatures are shown in Fig. 2. The XRD patterns of the samples can be readily indexed to tetragonal-type CuFe_2O_4 with $I41/AMD$ space group which is in agreement with ICDD card no. 34-0425 [6]. Identification of the structure type using the X'pert package confirms a spinel structure without the presence of impurity phases. As can be seen, upon increasing the temperatures, the Bragg angle ($35.9\text{-}36.3^\circ$) of the prominent peak (211) moves to lower angles.

Values of lattice parameters a and c obtained from Rietveld refinement implemented in the Fullprof program for CuF1, CuF2, and CuF3, are given in Table 1. However, the increase of the lattice parameter (a) and decrease in lattice parameter (c) with the calcination temperature is in agreement with those reported in Refs. [7, 8] as given in Table 1. It is due to the migration of larger Cu^{2+} ions from the tetrahedral site to the octahedral site which results in the decrease of inversion parameter and occurrence of a structural phase transition from tetragonal to cubic spinel structure [9]. Although CuFe_2O_4 ferrite calcined at 1000 °C in Ref. [9] shows a cubic spinel structure, we cannot observe any traces of cubic spinel structure for the CuF3 sample.

3.2. Determination of crystallite size, microstrain, and particle size

Below, a comparative study of the mean crystal sizes of CuF1, CuF2, and CuF3 obtained from the XRD powder pattern is reported. The microstrain due to lattice deformation CuF1, CuF2, and CuF3 nanoparticles was estimated by Williamson Hall (WH), size-strain plot (SSP), and Halder-Wagner (HW) methods, and the crystallite sizes results obtained by these methods are compared with the Scherrer methods. In all these methods, the values of β_{hkl} (the full-width at half-maximum (FWHM) of the diffraction peak) and θ are selected from the results obtained from X'pert High Score package. Also, the values of d_{hkl} (the distance between adjacent planes in the Miller indices (hkl)) are calculated from Bragg's equation, $2d_{hkl} \sin \theta = \lambda$, with $\lambda = 1.5404 \text{ \AA}$.

3.2.1. The Scherrer method

The instrumental corrected broadening [10] $\beta_{hkl} (= \beta_c)$ was estimated by using Gaussian function:

$$\beta_c^2 = \beta_{hkl}^2 = \beta^2 - \beta_i^2 \quad (2)$$

Also, Scherrer's equation is as follows [11]:

$$\beta_{hkl} = \frac{K\lambda}{D \cos \theta} = \beta_c \quad (3)$$

Table 1The 2θ and β_{hkl} values of (211) diffraction peak and the crystallite size obtained from the Scherrer method for CuF1, CuF2, and CuF3

Samples	a (Å)	c (Å)	a (Å)	c (Å)	(hkl)	2θ (°)	β _{hkl} (°)	D Scherrer (nm)
CuF1	5.7683	8.6812	5.830 [7]	8.662 [7]	(2 1 1)	36.31	0.4869	17.94
CuF2	5.7920	8.6786	5.832 [7]	8.660 [7]	(2 1 1)	36.17	0.4658	18.74
CuF3	5.8169	8.6686	8.239 [8]	8.724 [8]	(2 1 1)	36.03	0.2325	37.54

show the broadening of the XRD pattern which is attributed to the crystallite size (D) -induced broadening. Here, β_{hkl} and θ are the full-width at half maximum (FWHM) corresponding to the Bragg's angle of (211) peak of CuF1, CuF2, and CuF3 as shown in Fig. 2, respectively. The K, and λ are the Scherrer constants equal to 0.94, and the X-ray wavelength, respectively.

In this method, the increase in peak broadening is due to the reduction in crystallite size. The Scherrer formula uses Gaussian line profiles to determine the size of the crystallite. This formula is not expected to be valid for very small crystallite sizes (<10 nm). The crystallite size (D) of the samples was extracted from the Scherrer method as shown in Table 1. It should be noted that the crystallite sizes obtained from smaller diffraction angles are more accurate.

3.2.2. Williamson-Hall (W-H) method

In the W-H method, the information on microstrain (ε) and the crystallite size (D) of CuF1, CuF2, and CuF3 have been obtained from β_{hkl} by using W-H relation. Microstrain broadening in the W-H method is defined as follows [12]:

$$\beta_s = 4\varepsilon \tan \theta \quad (4)$$

Separating crystallite size broadening and microstrain broadening,

$$\beta_{hkl} = \beta_c + \beta_s = \left(\frac{K \lambda}{D \cos \theta} \right) + (4\varepsilon \tan \theta) \quad (5)$$

Rewriting Eq. (5), the formula for the Williamson-Hall method is as follow [13]:

$$\beta_{hkl} \cos \theta = \left(\frac{K \lambda}{D} \right) + (4\varepsilon \sin \theta) \quad (6)$$

where K is the Scherrer constant or the shape coefficient given as 0.94 for spherical particles and ε is the internal microstrain.

In this method, the plot of β_{hkl} cos θ (axis-y) versus 4 sin θ (axis-x) corresponding to the six strongest peaks of CuF1, CuF2, and CuF3 shown in Fig. 2, is a straight line (see Fig. 3 a). The slope and intercept of linearly fitted data give amounts of micro-strain (ε) and crystallite size D_{W-H}, respectively. The resulting negative microstrain may be caused by lattice contraction. Basically, the larger the interception result, the smaller the crystallite size, and the larger the slope, the larger the microcrack. Interruption

with origin means that D is infinite or broadening is only due to micro-strain dilation, and zero slope means that the horizontal line without micro-strain or broadening is only due to broadening of the crystallite size. The D_{W-H} value is incorrect due to the lower R² values.

The scattered data analyzed on plots of CuF1, CuF2, and CuF3 using the Williamson -Hall (W-H) method (shown in Fig. 3a) does not show any clear linear fitting behavior which shows this method is not more accurate. Since the W-H method supposes that “crystallite size” profile and the “microstrain” profile contribute to the line broadening with Lorentzian profiles, so it doesn't match with the X-ray broadening of the studied sample.

3.2.3. Size-Strain Plot method

The information on microstrain (ε) and the crystallite size (D) of CuF1, CuF2, and CuF3 have been obtained from β_{hkl} and planar spacing d_{hkl} (the distance between adjacent planes in the set (h k l)) by using a size-strain plot (SSP) method. The SSP method is more accurate, especially at higher diffraction angles. Therefore, the crystallite size and lattice strain of the sample were calculated using the SSP method. In this method, the peak broadening due to the lattice strain is estimated from ε = β_s/tan θ [14]. Therefore, the total broadening is obtained from:

$$\beta_{hkl} = \beta_c + \beta_s \quad (7)$$

According to the SSP method, the relation between lattice strain and crystallite size is given by [15]:

$$(d_{hkl} \beta_{hkl} \cos \theta)^2 = (K/D)(d_{hkl}^2 \beta_{hkl} \cos \theta) + (\varepsilon/2)^2 \quad (8)$$

where K is the shape coefficient given as 3/4 for spherical particles.

In the SSP method, the plot of (d_{hkl} β_{hkl} cos θ)² (axis y) versus (d_{hkl}² β_{hkl} cos θ) (axis-x) corresponding to the six strongest peaks of CuF1, CuF2, and CuF3 shown in Fig. 2, is a straight line (see Fig. 3 b). The size of the crystallite is determined by the slope of the linear fitting data and the root of the y-intercept gives the microstrain.

3.2.4. Halder-Wagner method

The information on microstrain (ε_{H-W}) and the crystallite size (D_{H-W}) of CuF1, CuF2, and CuF3 have been obtained from β_{hkl} and planar spacing d_{hkl} (the distance between adjacent planes in the set (h k l)) by using the H-W method.

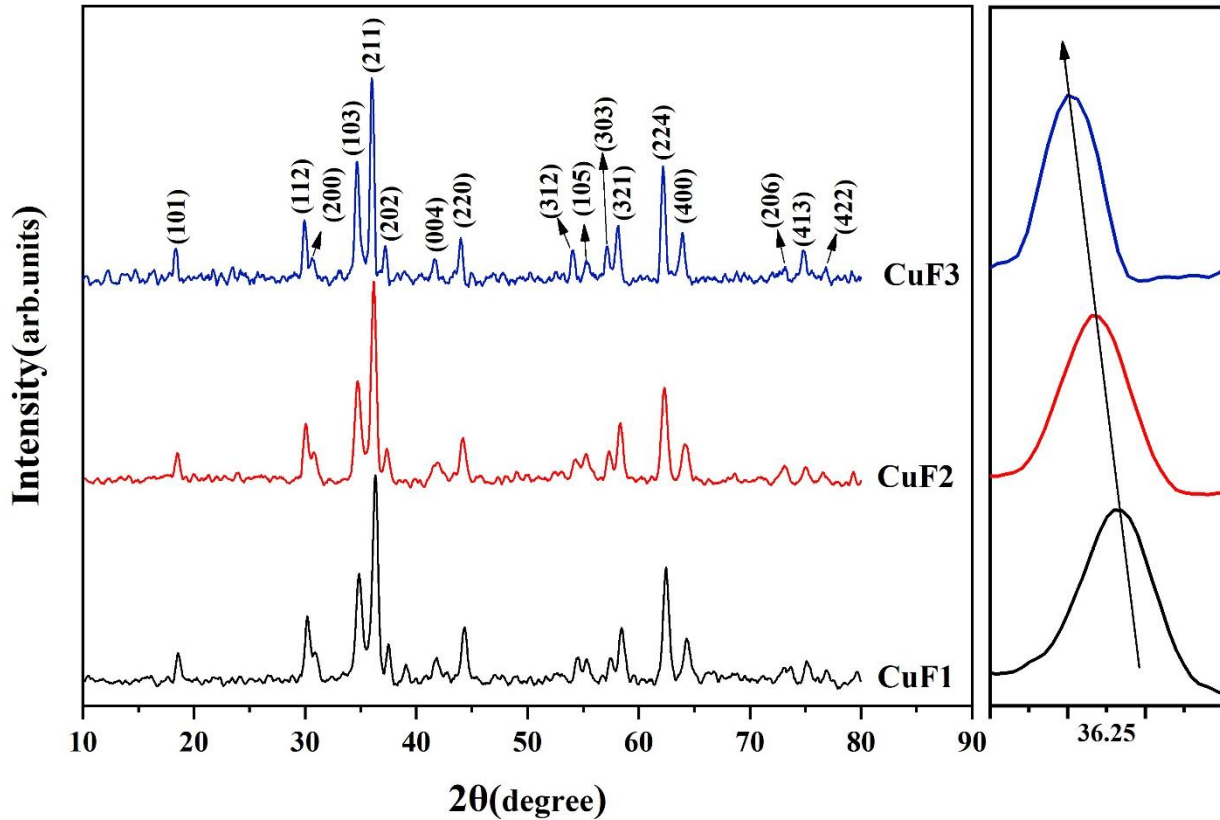


Fig. 2. X-ray diffraction pattern of CuFe_2O_4 ferrite was synthesized by the citrate precursor method and further calcined at 800 °C (CuF1), 900 °C (CuF2), and 1000 °C (CuF3)

Halder and Wagner have given an approximation to the integral breadth of a Voigt function as [16]:

$$\beta_{hkl}^2 = \beta_L \beta_{hkl} + \beta_G^2 \quad (9)$$

where β_L and β_G are the Lorentzian and Gaussian components, respectively. In the H-W method, the crystallite size and strain profiles are described by the Lorentzian and the Gaussian function, respectively. Consequently, we have [17]:

$$(\beta_{hkl}^*/d_{hkl}^*)^2 = (1/D)(\beta_{hkl}^*/d_{hkl}^*)^2 + (\varepsilon/2)^2 \quad (10)$$

$$\beta_{hkl}^* = \beta_{hkl} \cos\theta/\lambda \text{ and } d_{hkl}^* = 2\sin\theta/\lambda.$$

In the H-W method, the plot of $(\beta_{hkl}^*/d_{hkl}^*)^2$ (axis y) versus $(\beta_{hkl}^*/d_{hkl}^*)^2$ (axis-x) corresponding to the six strongest peaks of CuF1, CuF2, and CuF3 shown in Fig. 2, is a straight line with a positive slope and a nonzero y-intercept (see Fig. 3 c). The crystallite size is determined from the slope inverse of the linearly fitted data and the root of the y-intercept gives the microstrain, respectively.

The results of crystallite size and microstrain of CuF1, CuF2, and CuF3 estimated by Scherrer, W-H, SSP, and H-W methods are summarized in Table 2. All methods show that the line broadening was essentially isotropic. The WH method supposes that the "crystallite size" profile and the "microstrain" profile contribute to the line broadening with

Lorentzian profiles, but in both SS and HW methods the "crystallite size" profile is described by a Lorentz function and the "microstrain" profile by a Gaussian function. However, both of the S-S and H-W methods compared to Scherrer and W-H methods have the advantage that less weight is given to data from reflections at high angles, where the precision is usually lower. For this reason, in the W-H method is suggested that the smaller angle peaks should be used to separate β_c and β_s . In addition, the SSP and H-W methods give a high value of strain because of the contribution of low and mid-angle XRD data. Further, the calculated higher value of strain may be attributed to the lattice dislocations, which play a significant role in the broadening of the reflection peaks at lower angles.

The average size values of CuF1, CuF2, and CuF3 crystallites obtained from different models are less similar, implying that the inclusion of microstrains in different shapes has a substantial effect on the average crystallite size of CuF1, CuF2, and CuF3. However, take a look at the R^2 values written in the figure. 3 a-c, we can see that the SSP method is more accurate, with all the data points touching the fitting line. This method also has a minimum of microstrain. Thus, it is a more accurate method in which the value of R^2 is close to 1, or in other words, the data points x-y touch the fitting line more.

The crystallite size of the CuFe_2O_4 ferrite increased from ~8.0 nm to ~11.8 nm with increasing the calcination temperature from 800 °C to 1000 °C due to faster recrystallization and grain growth of ferrite. However, the results given in Table 2 suggest that in the investigated ferrites, the increase of the crystallite sizes with calcination

temperature can be mainly attributed to the increase of stretching microstrain.

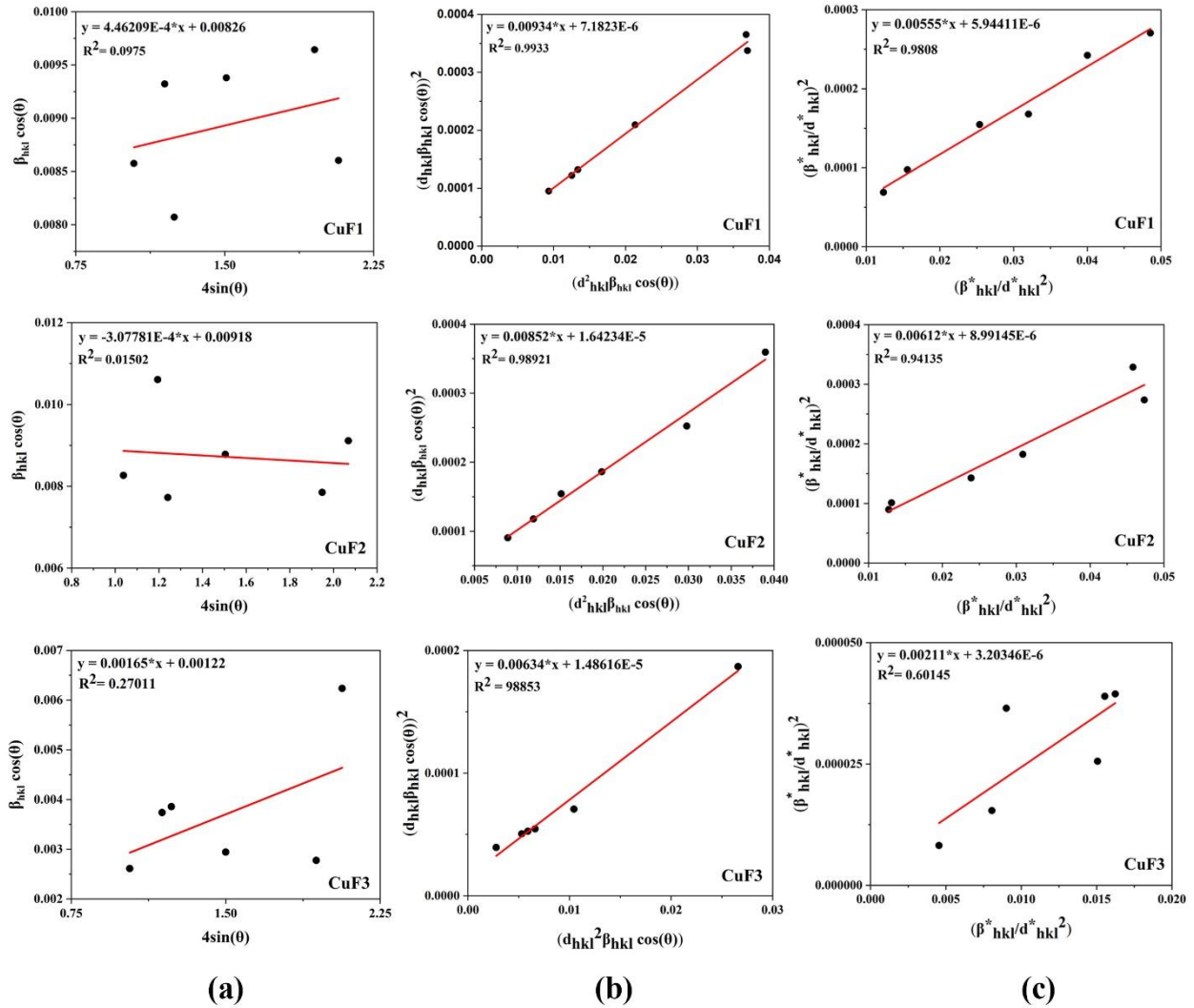


Fig. 3. The W-H (a), SSP (b), and H-W (c) plots for CuF1, CuF2, and CuF3

Table 2

The values of crystallite size and microstrain of CuF1, CuF2, and CuF3 obtained from Williamson-Hall (W-H) analysis, size-strain plot (SSP), and Halder-Wagner (H-W) methods.

Samples	D_{W-H} (nm)	ϵ_{W-H} (no unit) *10 ³	D ssp (nm)	$\epsilon_{SSP} * 10^3$ (no unit)	D_{H-W} (nm)	ϵ_{H-W} (no unit) *10 ³
CuF1	17.52	0.44	8.03	5.36	18.00	4.88
CuF2	15.76	-0.30	8.46	6.15	16.33	6.00
CuF3	118.52	1.65	11.83	7.71	47.29	3.58

4. Conclusion

The structural characterization of CuF1, CuF2, and CuF3 prepared by citrate technique is investigated by X-ray powder diffraction. The results of the X'Pert package are evidence for a CuFe₂O₄ structure with *I* 41/*AMD* space group. The results of crystallite size and microstrain estimated by the Scherrer, W-H, SSP, and H-W methods for CuF1, CuF2, and CuF3 samples show the SSP method is more accurate, which the value of R² is near 1 with all data points touching the fitting line better than the other methods.

References

- [1] Y. Slimani, M.A. Almessiere, A. Demir Korkmaz, S. Guner, H. Güngüneş, M. Sertkol, A. Manikandan, A. Yildiz, S. Akhtar, Sagar E. Shirsath, A. Baykal, Ni_{0.4}Cu_{0.2}Zn_{0.4}Tb_xFe_{2-x}O₄ nanospinel ferrites: Ultrasonic synthesis and physical properties, Ultrason. Sonochem. 59 (2019) 104757.
- [2] R.S. Yadav, J. Havlica, J. Masilko, L. Kalina, J. Wasserbauer, M. Hajd'uchov'a, V. Enev, I. Ku'ritk, Z. Ko'z'akov'a, Cation Migration-Induced Crystal Phase Transformation in Copper Ferrite Nanoparticles and

- Their Magnetic Property, *J. Supercond. Nov. Magn.* 29 (2016) 759–769.
- [3] H. Hou, G. Xu, S. Tan, Y. Zhu, A facile sol-gel strategy for the scalable synthesis of CuFe_2O_4 nanoparticles with enhanced infrared radiation property: Influence of the synthesis conditions, *Infrared Phys. Technol.* 85 (2017) 261–265.
- [4] R. Yogamalara, R. Srinivasan, A. Vinu, K. Ariga, A. C. Bose, X-ray peak broadening analysis in ZnO nanoparticles, *Solid State Commun.* 149 (2009) 1919–1923.
- [5] A. Khorsand Zak, W.H. Abd. Majid, M.E. Abrishami, R. Yousefi, X-ray analysis of ZnO nanoparticles by Williamson-Hall and size-strain plot methods, *Solid State Sci.* 13 (2011) 251–256.
- [6] H. Yang, J. Yan, Z. Lu, X. Cheng, Y. Tang, Photocatalytic activity evaluation of tetragonal CuFe_2O_4 nanoparticles for the H_2 evolution under visible light irradiation, *J. Alloys Compd.* 476 (2009) 715–719.
- [7] J. Calvo-de la Rosa, M. Segarra Rubí, Influence of the Synthesis Route in Obtaining the Cubic or Tetragonal Copper Ferrite Phases, *Inorganic Chemistry* 59 (2020) 8775–8788.
- [8] M.J. Iqbal, N. Yaqub, B. Sepiol, B. Ismail, A study of the influence of crystallite size on the electrical and magnetic properties of CuFe_2O_4 , *Mater. Res. Bull.* 46 (2011) 1837–1842.
- [9] D. Thapa, N. Kulkarni, S.N. Mishra, P.L. Paulose, P. Ayyub, Enhanced magnetization in cubic ferrimagnetic CuFe_2O_4 nanoparticles synthesized from a citrate precursor: the role of Fe^{2+} , *J. Phys. D: Appl. Phys.* 43 (2010) 195004.
- [10] K. D. Rogers, P. Daniels, An X-ray diffraction study of the effects of heat treatment on bone mineral microstructure, *Biomaterials* 23 (2002) 2577.
- [11] A. Gholizadeh, A comparative study of physical properties in Fe_3O_4 nanoparticles prepared by coprecipitation and citrate methods, *J. Am. Ceram. Soc.* 100 (2017) 3577–3588.
- [12] A. R. Stokes, A. J. C. Wilson, The diffraction of X rays by distorted crystal aggregates –I, *Proc. Phys. Soc.* 56 (1944) 174.
- [13] G. K. Williamson, W. H. Hall, X-RAY LINE BROADENING FROM FILED ALUMINIUM AND WOLFRAM, *Acta Metall.* 1 (1953) 22.
- [14] B. D. Cullity, *Elements of X-ray Diffraction*, Addison-Wesley Publishing Company Inc., California, 1956.
- [15] M.A. Tagliente, M. Massaro, Strain-driven (002) preferred orientation of ZnO nanoparticles in ion-implanted silica, *Nucl. Instrum. Methods. B* 266 (2008) 1055–1061.
- [16] N.C. Halder, N.C.J. Wagner, Separation of particle size and lattice strain in integral breadth measurements, *Acta Crystallogr.* 20 (1966) 312.
- [17] J. E. Langford, *International Conference Accuracy in Powder Diffraction II*, National Institut of Standards and Technology, Special Publication, Gaithersburg, MD, USA, 846 (1992) 145.